International Journal of Minerals, Metallurgy and Materials
Volume 20, Number 7, July 2013, Page 620
DOI: 10.1007/s12613-013-0775-7

Mathematical model of burden distribution for the bell-less top of a blast furnace

Zhao-jie Teng[1)], *Shu-sen Cheng*[1)], *Peng-yu Du*[2)], *and Xi-bin Guo*[3)]

1) State Key Laboratory of Advanced Metallurgy, University of Science and Technology Beijing, Beijing 100083, China

2) MCC Capital Engineering and Research Incorporation Limited, Beijing 100176, China

3) Xuanhua Iron and Steel Company, Xuanhua 075100, China

(Received: 8 August 2012; revised: 12 September 2012; accepted: 17 September 2012)

Abstract: Due to the difficulty in measuring the burden trajectory directly in an actual blast furnace (BF), a mathematical model with Coriolis force and gas drag force considered was developed to predict it. The falling point and width of the burden flow were obtained and analyzed by the model, the velocities of particles at the chute end were compared with and without the existence of Coriolis force, and the effects of chute length and chute torque on the falling point were also discussed. The simulation results are in good agreement with practical measurements with laser beams in a 2500 m^3 BF.

Keywords: blast furnaces; burden; trajectories; mathematical models; Coriolis force

1. Introduction

In recent years, the burden distribution has received much attention due to its importance to the smooth operation of a blast furnace (BF) [1-2]. The distribution of burden materials can influence the radial ore/coke ratio, size segregation, burden descent, and gas distribution, which in turn affect the shape of the cohesive zone [3-4]. In order to predict the burden distribution, the movement of raw particles should be analyzed for a bell-less top.

The movement of raw particles includes moving in the chute and falling in the freeboard. There are already some mathematical models concerning the burden distribution [5-11], but most of them have not considered the effect of Coriolis force. Coriolis force is a force that makes an object move with direction migration because of inertia when the object moves in a straight line in a rotating system. Nag and Koranne [12] described the movement of a particle in the chute with Coriolis force, but the effect of gas flow was ignored, and the width of burden flow was not calculated. Mio *et al.* [13] found that the stock profile of burden flow at different cross sections changed in the rotating chute with Coriolis force by discrete element method (DEM), but the burden distribution has not been calculated quantitatively.

In this paper, a mathematical model was established to analyze particles movement in the chute and the freeboard, and the width of burden flow was calculated. In order to validate the model, the trajectory and the width of burden flow were measured in an actual 2500 m^3 BF of Xuanhua Iron and Steel Co. Ltd., China by laser equipment. With the mathematical model, the trajectories of particles and the width of burden flow can be estimated.

2. Model development

2.1. Flow through rotating chute

The movement of a particle in a rotating chute can be obtained through analyzing forces acting on the particle. Fig. 1 shows a particle moving in a chute, in which G ($G = mg$) is the gravitational force, F_T ($F_T = 4\pi^2 z\omega^2 sin\alpha m$) is the centrifugal force, F_N is the supporting force, $F_k(\overrightarrow{F}_k = 2m\overrightarrow{v} \times \overrightarrow{\omega})$ is the Coriolis force, N is the normal pressure force, and $F_f(F_f = \eta N)$ is the frictional force. The direction of Coriolis force is towards right if the chute rotates clockwise, so the particle can move along the tangential direction of the chute simultaneously.

The movement of a particle in the rotating chute can be described in three directions. z coordinate is the direction along the chute, and x and y coordinates are shown in the cross section of the chute. Analyzing the forces focus-

Corresponding author: Zhao-jie Teng E-mail: tengzhaojie2012@163.com

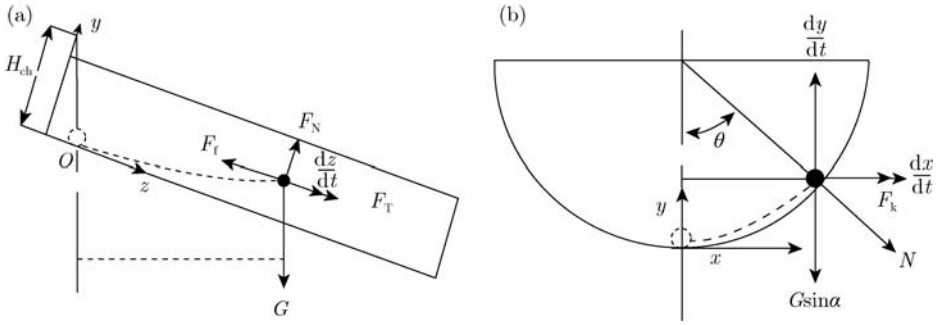

Fig. 1. Movement of a particle in the chute: (a) chute longitudinal direction; (b) chute cross section.

ing on the particle, the mathematical model of the particle movement is established.

$$\frac{\mathrm{d}^2z}{\mathrm{d}t^2} = g\cos\alpha + \omega^2[z\sin\alpha - (R-y)\cos\alpha]\sin\alpha - 2\omega\sin\alpha\frac{\mathrm{d}x}{\mathrm{d}t} - \eta\frac{\frac{\mathrm{d}z}{\mathrm{d}t}}{mv}N \quad (1)$$

$$\frac{\mathrm{d}^2x}{\mathrm{d}t^2} = \omega^2x + 2\omega\sin\alpha\frac{\mathrm{d}z}{\mathrm{d}t} - \eta\frac{\frac{\mathrm{d}x}{\mathrm{d}t}}{mv}N \quad (2)$$

$$\frac{\mathrm{d}^2y}{\mathrm{d}t^2} = -g\sin\alpha + \omega^2[z\cos\alpha - (R-y)\cos\alpha] - \eta\frac{\frac{\mathrm{d}y}{\mathrm{d}t}}{mv}N \quad (3)$$

$$N = m\Bigg[g\sin\alpha\cos\theta + \omega^2R - \omega^2\cos\theta\sin\alpha(z\cos\alpha + R\cos\theta\sin\alpha) + 2\omega R\cos\alpha\frac{\mathrm{d}\theta}{\mathrm{d}t} + 2\omega\sin\alpha\sin\theta\frac{\mathrm{d}z}{\mathrm{d}t} + R\left(\frac{\mathrm{d}\theta}{\mathrm{d}t}\right)^2\Bigg] \quad (4)$$

$$\tan\theta = \frac{x}{R-y} \quad (5)$$

$$\nu = \left[\left(\frac{\mathrm{d}x}{\mathrm{d}t}\right)^2 + \left(\frac{\mathrm{d}y}{\mathrm{d}t}\right)^2 + \left(\frac{\mathrm{d}z}{\mathrm{d}t}\right)^2\right]^{\frac{1}{2}} \quad (6)$$

where m is the particle mass, kg; g is the gravitational acceleration, m/s^2; α is the chute inclination angle, (°); η is the friction coefficient; ω is the angular velocity, rad/s; H_{ch} is the chute torque, m; L is the chute length, m; v is the particle velocity in the chute, m/s; R is the chute radius, m; and θ is the moved angle in the tangential direction, (°).

Based on Eqs. (1)-(6), the velocity and position of the particle at the chute end can be obtained using the fourth order Runge-Kutta method. The velocity at the chute end can affect the movement in the freeboard.

2.2. Drop from the chute end

The particle will descend in the freeboard after it moves out of the chute. The moving process is shown in Fig. 2, and the falling point can be calculated from the values of horizontal and vertical components of the particle velocity. When a particle moves in the freeboard, it will be affected by the gravitational force, drag force, and the buoyancy force.

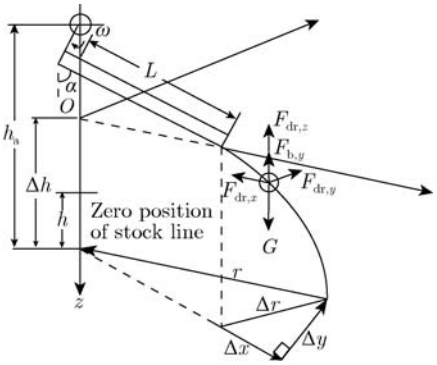

Fig. 2. Particle movement below the chute end.

The particle descending in the freeboard can be described within x, y, and z coordinates. In z coordinate, the forces acting on particles are the gravitational force $G\,(G = mg)$, the buoyancy force $F_{b,y}\,(F_{b,y} = \rho_g g V_p)$, and drag force $F_{dr,z}\,(F_{dr,z} = C(\nu_z - \nu_{g,z})^2)$. The movement of the particle can be described as

$$m\frac{\mathrm{d}\nu_z}{\mathrm{d}t} = mg - C(\nu_z - \nu_{g,z})^2 - \rho_g g V_p \quad (7)$$

In y coordinate, the dominant force is drag force $F_{dr,y}\,(F_{dr,y} = -C(\nu_y - \nu_{g,y})^2)$, and then the movement equation can be expressed as

$$-m\frac{\mathrm{d}\nu_y}{\mathrm{d}t} = C(\nu_y - \nu_{g,y})^2 \quad (8)$$

In the x coordinate, drag force is $F_{dr,x} = -C(\nu_x - \nu_{g,x})^2$, then

$$-m\frac{\mathrm{d}\nu_x}{\mathrm{d}t} = C(\nu_x - \nu_{g,x})^2 \quad (9)$$

The coefficient of the drag force is given as follows:

$$C = \frac{1}{2}\left[\frac{24}{Re}(1 + b_1Re^{b_2}) + \frac{b_3Re}{b_4 + Re}\right]\frac{\pi d^2}{8}\rho_g \quad (10)$$

$$\begin{cases} b_1 = \exp(2.3288 - 6.4581\phi + 2.4486\phi^2) \\ b_2 = 0.0964 + 0.5565\phi \\ b_3 = \exp(4.905 - 13.8944\phi + 18.4222\phi^2 - 10.2599\phi^3) \\ b_4 = \exp(1.4681 + 12.2584\phi - 20.7322\phi^2 + 15.8855\phi^3) \end{cases},$$

$$Re = \frac{\rho_g d|\nu - \nu_g|}{\mu_g},$$

where C is the gas drag force coefficient; ρ_g is the gas density, kg/m^3; ν_z is the particle velocity at the chute end in z coordinate, m/s; $\nu_{g,z}$ is the gas flow velocity in z coordinate, m/s; V_p is the particle volume, m^3; ν_y is the particle velocity at the chute end in y coordinate, m/s; $\nu_{g,y}$ is the gas flow velocity in y coordinate, m/s; ν_x is the particle velocity at the chute end in x coordinate, m/s; $\nu_{g,x}$ is the gas flow velocity in x coordinate, m/s; d is the particle diameter, m; μ_g is the gas viscosity coefficient, Pa·s; ϕ is the shape fraction.

In order to calculate the falling point, the falling time should be calculated. The falling time is determined by the height of the fall distance and the velocity of the particle in the $z$coordinate. The height of the particle moving in freeboard Δh is as follows:

$$\Delta h = h_a - H_{ch}/\sin\alpha - (L - H_{ch}/\tan\alpha)\cos\alpha \quad (11)$$

Using Eqs. (1)-(11), the distance r of the falling point from the BF center can be calculated. Since the velocity varied with time in the freeboard, Δh can be divided into n sections, and the velocity can be seen as a constant in the small section. The moving time in each section can be calculated, and then, the moving distance in x and y coordinates can be obtained. The moving distance Δx and Δy in the x and y coordinates can be obtained after the particle moves n section in z coordinate. The distance of the falling point r can be calculated from Eq. (12).

$$r = \sqrt{(L\sin\alpha + \Delta x)^2 + \Delta y^2} \quad (12)$$

2.3. Width of burden flow

Burden flow can be regarded as a set of numerous particles. While using the mathematical model to analyze the burden distribution, for the simplification of calculation, collision of the particles was ignored, and the movement of all particles was assumed to be the same. Then, the burden flow trajectory can be regarded as one particle trajectory.

When particles move along a rotating chute (longitudinal direction), the particles also move in the tangential direction because of the influence of Coriolis force. Fig. 3 shows the effect of Coriolis force on the stock profile of burden flow in the chute when the chute rotates clockwise. The profile of burden flow corresponds to the dot line and the height is h_{db} without Coriolis force been considered, but the profile corresponds to the solid line, and the height is h_{rb} in the actual process. The height of burden flow in the chute increases. The burden flow width is shown in Fig. 4. The increase in height of burden flow makes the width of burden flow in the BF change.

$$S = \frac{Q}{\rho\nu_a} = \frac{R^2}{2}(\varphi - \sin\varphi) \quad (13)$$

$$h_{rb} = R - R\cos(\frac{\varphi}{2} + \theta) \quad (14)$$

where S is the sectional area of burden along the chute, m^2; Q is the mass flow rate of burden, kg/s; ρ is the solid density, kg/m^3; and φ is the field angle of burden width when falling to the chute, (°).

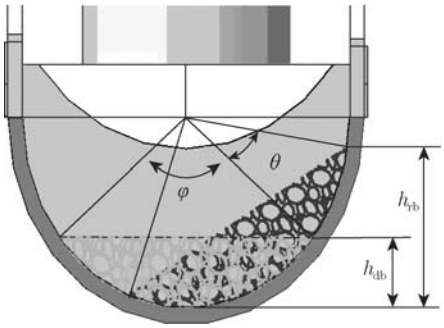

Fig. 3. Effect of Coriolis force.

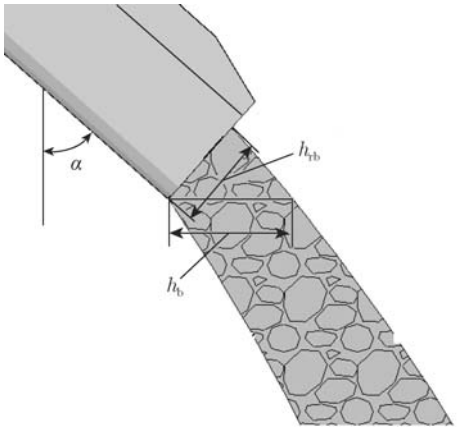

Fig. 4. Width of burden flow.

3. Plant trials

Experiments were conducted using actual bell-less top charging equipment in a blast furnace to validate the mathematical model. The BF parameters are listed in Table 1, and the physical properties of raw materials are listed in Table 2. The friction coefficient can be measured when particles drop on an oblique plate with 30°, and the moving distance can also be measured [14].

With the purpose of measuring the burden trajectory in an actual BF, laser equipment has been used, which

Table 1. Parameters of the BF top

Chute length / m	Chute rotating speed / (rad · s^{-1})	Chute radius / m	Distance between point hanging chute and chute liner, H_{ch} / m	Distance between chute hanging point and zero stock level / m
4.02	0.125	0.44	0.77	5.78

Table 2. Physical properties of raw materials

Materials	Bulk density / (kg·m^{-3})	Shape factor	Friction coefficient	Diameter / mm
Coke	550	0.72	0.5	56.7
Sinter	1670	0.44	0.6	15.7
Pellet	1960	0.92	0.2	12.7

emit beams. The laser beams used in the experiment are shown in Fig. 5. There were 42 laser beams installed at two sides of the BF in total, and the meshes were generated in the BF to set up a grid system. The angle between every two laser beams was kept to be constant, and the position of each line can be known if the installation position of lasers is determined. Each intersection of the mesh corresponds to the BF constant position. When the particles move out of the chute and descend in the freeboard, the trajectories could be known from the laser beam meshes.

With the application of laser beams, the burden flow trajectories were recorded by a charged-coupled device (CCD) camera. From images from CCD camera, the trajectory of burden flow can be obtained. Fig. 6 shows the burden trajectories in an actual BF. Using the coordinate system set up by laser beams, each point position in the BF can be obtained. When the burden moves through laser beam meshes, the trajectory of burden flow can be known. The analyzed process of the laser measured images can be estimated from Ref. [15].

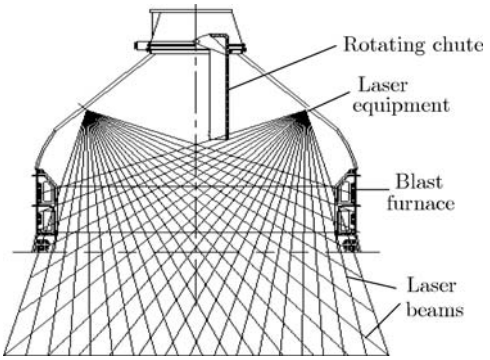

Fig. 5. Distribution of the laser beams.

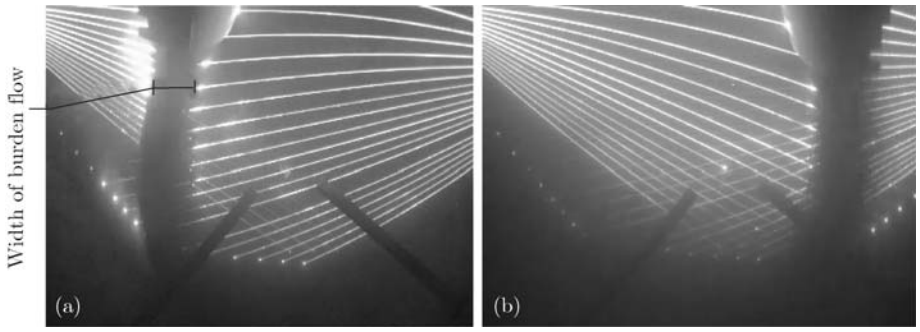

Fig. 6. Trajectory of burden flow in the BF: (a) $\alpha = 36°$; (b) $\alpha = 34°$.

4. Results and discussion

4.1. Trajectory of burden flow

The mathematical model can predict the radial falling position of coke and metallic materials at a given stock level with different chute inclination angles. With the laser meshes and the CCD camera, the trajectories of burden flow can be measured. Fig. 7 shows both the measured and the calculated falling point with different chute inclination angles at the stock line of 1 m and 2 m for cokes, respectively. For the BF blow-out, the falling point of particles has been measured and calculated without gas flow been considered. As the burden flow strikes the stock level with a width of 0.45-0.65 m, the distance of the mid-position of the burden flow from the centerline is considered as the falling point. It is noted that although there are some differences between the calculated results and measured results, since the value of particle size used in this model is the averaged value and the measurement error has been considered, overall, the calculated results show good agreement with the measured results.

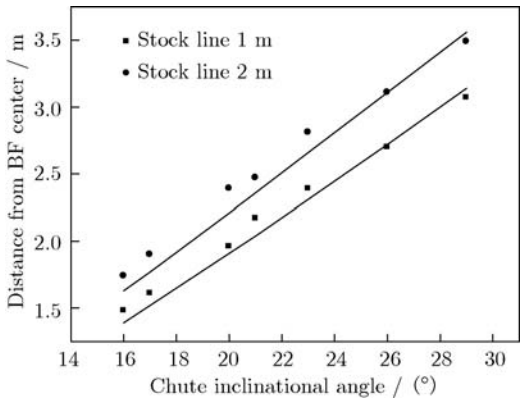

Fig. 7. Falling point of the measured result (dot) and the calculated result (solid line).

Fig. 7 indicates that the falling point moves toward the BF wall with the inclinational angle increasing. The relationship between the falling point and the inclinational angle is $Y = 0.1222X - 0.3504$. The distance of the falling point extends 0.122 m when the chute inclinational angle increases by 1°.

The width of burden flow can be obtained from the result of the trajectories by laser beams. Fig. 8 shows the measured widths and the calculated widths of burden flow with different stock lines. The results show that the width of burden flow increases with the increase of the stock line and chute inclination angle. In this BF, the width of burden flow is 0.45-0.65 m. It could be found that the calculated results can be used to predict the actual flow of burden in a BF. The width of burden flow can also be calculated by the present mathematical model.

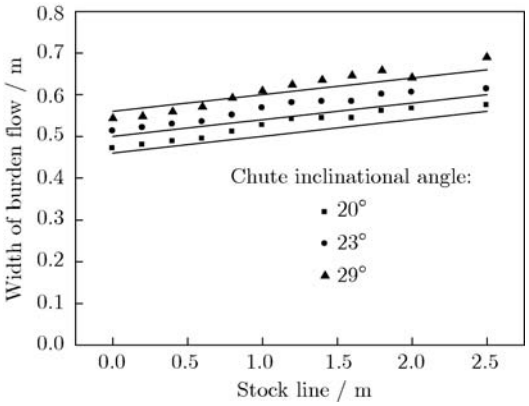

Fig. 8. Measured widths (dot) and calculated widths (solid line) of burden flow.

4.2. Effect of Coriolis force on the burden trajectory

Coriolis force will be generated when the chute rotates, and its direction is normal to the chute inside wall, which will result in changes of the burden stock profile in different cross sections.

From discussion above, it can be concluded that Coriolis force has a significant influence on the particle movement. Coriolis force affects the frictional force obviously. If it is ignored, the velocity of particles will be overestimated. A comparison with and without Coriolis force is shown in Fig. 9. It can be seen that without Coriolis force, the velocity of particles at the chute ends is up to 0.7 m/s higher than the result obtained with Coriolis force.

Coriolis force can affect the width of burden flow, the velocity of particles at the chute end, and the distance of the falling point. If Coriolis force is ignored, the analyzed results cannot be reasonable.

4.3. Effect of gas flow on the burden trajectory

Generally, particle size and gas flow velocity can influence the behavior of particles. The effect can be ignored if the particle size is large enough, but for small particles, the effect of gas flow is remarkable. Fig. 10 shows the effect of gas flow velocity on the particle distance of the falling point from the BF center. The coke size is 15 mm, the chute angle is 30°, and the velocity of gas flow is set to be 2, 4, 6, 8, and 10 m/s. For different velocities of gas flow, the drag force changes. As the drag force increases with the velocity of gas flow increasing, the particles tend to move to the BF wall at large gas velocity. Fig. 11 il-

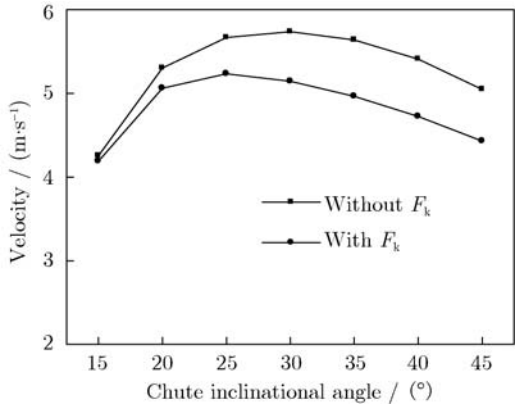

Fig. 9. Effect of Coriolis force on the velocity of particles.

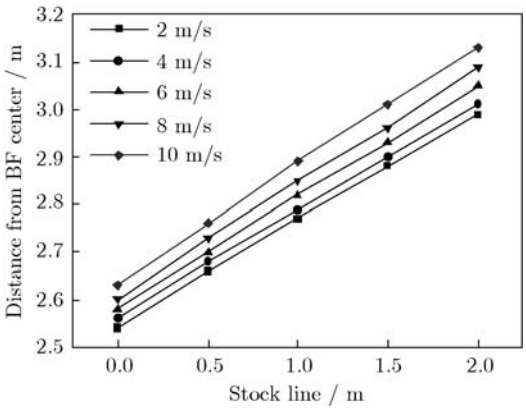

Fig. 10. Effect of gas flow velocity on the falling point.

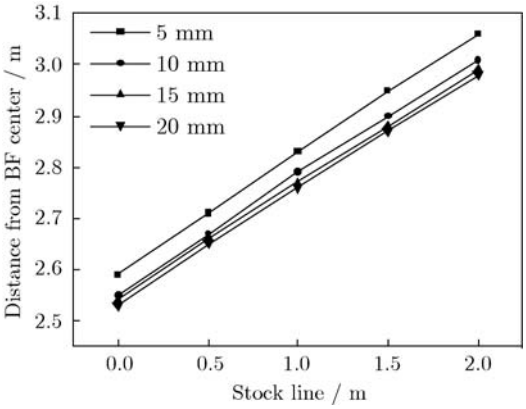

Fig. 11. Effect of particle size on the falling point.

lustrates the effect of particle size on the distance of the falling point from the BF center. The effect on smaller particles is much more remarkable. The falling point of particles with the diameter of 5 mm is farther, while the falling points of particles with the diameters of 10, 15, and 20 mm are nearly the same.

4.4. Effect of equipment parameters on the burden trajectory

It can be concluded that the burden trajectory can be affected by chute length and chute torque. The chute inclinational angle is 30° in the calculation of the falling point. Fig. 12 illustrates the effects of chute length on the falling point for sinters, pellets, and coke. The physical properties of raw materials are shown in Table 2. Fig. 12 shows that the distance from the falling point to the center increases when the chute becomes longer. When the chute length increases by 0.2 m, the falling point extends about 0.02 m.

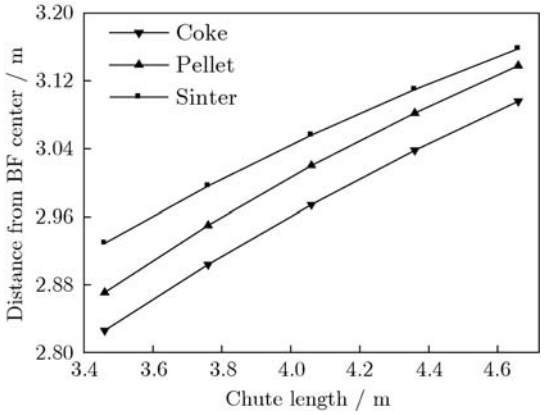

Fig. 12. Effect of chute length on the falling point.

Fig. 13 illustrates the effects of chute torque on the falling point for sinters, pellets, and coke. The distance of the falling point increases with the chute torque increasing. The relationship between the falling point and the chute torque is $Y = 3.854 - 1.14571X$. When the chute torque increases by 0.1 m, the distance of the falling point from the BF center will decrease by 0.115 m. Chute torque has a great effect on the burden trajectory.

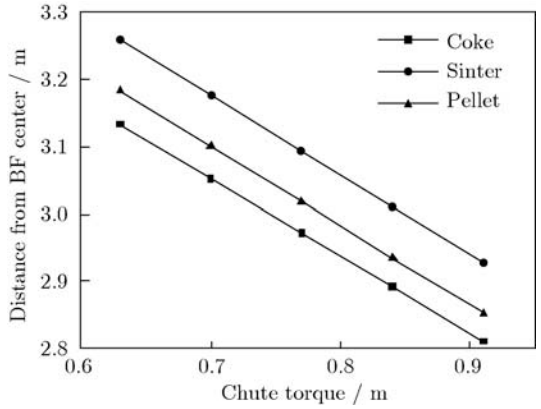

Fig. 13. Effect of chute torque on the falling point.

5. Conclusions

(1) The mathematical model was well validated by experimental data available. It can be used for determining the trajectory of coke and ores for any inclination angle over the entire range of operating stock levels.

(2) Coriolis force can increase friction between particles, thus affecting the speed of particles at the chute outlet. Whether there is Coriolis force or not, the particle speeds have significant difference, and Coriolis force also affect the stock profile of burden flow in the chute.

(3) Gas flow can affect the trajectory and delay the particle falling down. With the gas flow increasing, the falling point will move toward the BF wall. The effect of gas flow is more remarkable when the particle size is smaller.

(4) The falling point can be affected by chute length and chute torque when the chute length increases or the chute torque decreases, with the falling point moving toward the BF wall.

Acknowledgements

The authors would like to thank the Iron Works of Xuanhua Iron and Steel Company for giving the chance and help to measure the burden trajectory in its 2500 m^3 BF. This work was financially supported by the National Natural Science Foundation of China (No. 61271303).

References

[1] S. Ueda, S. Natsui, H. Nogami, J.I. Yagi, and T. Ariyama, Recent progress and future perspective on mathematical modeling of blast furnace, *ISIJ Int.,* 50(2010), No. 7, p. 914.

[2] J.I. Park, U.H. Baek, K.S. Jang, H.S. Oh, and J.W. Han, Development of the burden distribution and gas flow model in the blast furnace shaft, *ISIJ Int.,* 51(2011), No. 10, p. 1617.

[3] B.D. Pandey and U.S. Yadav, Blast furnace performance as influenced by burden distribution, *Ironmaking Steelmaking,* 26(1999), No. 3, p. 187.

[4] M. Hattori, B. Iino, A. Shimomura, H. Tsukiji, and T. Ariyama, Development of burden distribution simulation model for bell-less top in large blast furnace and its application, *ISIJ Int.,* 33(1993), No. 10, p. 1070.

[5] Q.T. Zhu and S.S. Cheng, Mathematical model of burden trajectory in a blast furnace, *J. Univ. Sci. Technol. Beijing*, 29(2007), No. 9, p. 932.

[6] Y.W. Yu, C.G. Bai, D. Liang, F. Xia, and W.J. Niu, A Mathematical model for bell-less top charging, *Iron Steel*,

43(2008), No. 11, p. 26.

[7] P.Y. Du, S.S. Cheng, Z.R. Hu, and T. Wu, Mathematical model of burden width in a bell-less top blast furnace and modeling experimental research, *Iron Steel*, 45(2010), No. 1, p. 14.

[8] P.Y. Du, S.S. Cheng, and Z.J. Teng, Measurement of charging trajectory in bell-less top burden of blast furnace and 3-D image reconstruction, *Metall. Ind. Autom.*, 33(2009), No. 6, p. 1.

[9] P. Wang, Measurement and analysis of burden flow trajectory and width in bell-less top with two concentric vertical hoppers, *Iron Steel*, 28(2003), No. 3, p. 8.

[10] Y. Matsui, A. Kasai, K. Ito, T. Matsuo, S. Kitayama, and N. Nagai, Stabilizing burden trajectory into blast furnace top under high ore to coke ratio operation, *ISIJ Int.,* 43(2003), No. 8, p. 1159.

[11] V.R. Radhakrishnan and K.M. Ram, Mathematical model for predictive control of the bell-less top charging system of a blast furnace, *J. Process Control*, 11(2001), No. 5, p. 565.

[12] S. Nag and V.M. Koranne, Development of material trajectory simulation model for blast furnace compact bell-less top, *Ironmaking Steelmaking*, 35(2009), No. 5, p. 371.

[13] H. Mio, S. Komatsuki, M. Akashi, A. Shimosaka, Y. Shirakawa, J. Hidaka, M. Kadowaki, S. Matsuzaki, and K. Kunitomo, Effect of chute angle on charging behavior of sintered ore particles at bell-less type charging system of blast furnace by discrete element method, *ISIJ Int.*, 49(2009), No. 4, p. 479.

[14] H. Mio, S. Komatsuki, M. Akashi, A. Shimosaka, Y. Shirakawa, J. Hidaka, M. Kadowaki, S. Matsuzaki, and K. Kunitomo, Validation of particle size segregation of sintered ore during flowing through laboratory-scale chute by discrete element method, *ISIJ Int.,* 48(2008), No. 12, p. 1696.

[15] P.Y. Du and S.S. Cheng, Laser measurement and image analysis of blast furnace bell-less top charging, *J. Univ. Sci. Technol. Beijing*, 32(2010), No. 1, p. 20.